本研究計画では、ブタを対象とした生体イメージング手法により、生体内での生理学的・病理学的状態をゲノム・エピゲノム・一分子レベルで可視化・理解し、従来の分子生物学的知見との整合性を検討する。特に、実際に機能が時間経過とともにゆらいでいると考えられる遺伝子のダイナミックな変化についてリアルタイムでの可視化を行い、「よりリアルな遺伝子機能」の可視化・定量化をめざす。

特に、本計画では、マウスとヒトの間にある大きなギャップをうめるために、ヒトにおける細胞・遺伝子機能の可視化にむけて、基礎技術開発を行い、生物学的な基礎的・応用的知見を得る生体に特化した顕微鏡の開発を行い、関連技術の特許取得をめざす。

本邦の死因の上位を占める生活習慣病では、臨床イベント発症前よりも、慢性炎症を基盤とする細胞動態・細胞間相互作用の異常が生じていると考えられる。たとえば、脳・心血管障害の多くは動脈硬化を基盤とした血栓性疾患であり、心血管イベントは確率的に生体内で動脈硬化巣の粥腫が破綻して起きると考えられるが、イベント以前より血管内皮障害や異常な血小板活性化が生じていると予測される。これらの、生活習慣病の前疾患状態を、光を用いて無侵襲に診断できれば、臨床的なインパクトはきわめて大きいと思われる。そこで、本研究計画では、今まで申請者が独自に開発してきたマウス生体光分子イメージング手法を大型動物の血管に適応する。心血管障害の発症前状態、糖尿病や肥満といった代謝性疾患をとらえるデバイスを開発する。本手法により基礎的に病態メカニズムを解明するのみならず、イベント発症予測や無侵襲な治療計画の決定に役立つ、新たな臨床診断手法の樹立をめざす。

B. 研究方法

(1) 生体イメージングシステムの開発

申請者は多分野の技術を統合し、全く新しい、高速・深部・高解像度の生体イメージング技術を開発し、生体における生体内の細胞動態を解析し、さらに、マウスレベルのシステムをブタへの応用を試みている。通常の顕微鏡が用いられないために、倒立の顕微鏡ユニットを用いた。観察系としては、二光子顕微鏡は光路を維持することが困難であることから、一光子共焦点顕微鏡を最初の目標とした。ブタ血管での高速・two color イメージングをめざして、横河電機社CSU-X1(スピニング・ニポウ式)を使用することとした。カメラは 2nd ポートを用いて、Andor 社 iXon を 2 台用いることとした。光源は、ダイオードレーザーとし、405、488、568 nm の三波長とし、フィルターホイールを用いて制御することとした。システム図は下記の通りである(**図 1**、**図 2**)。
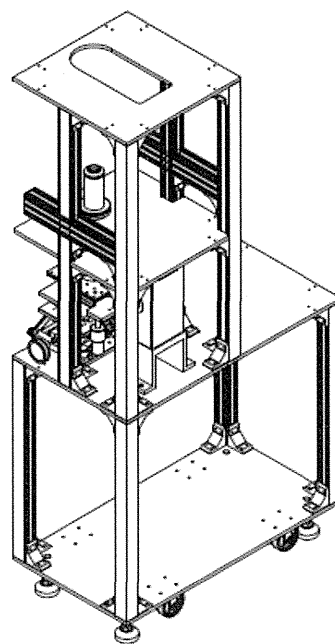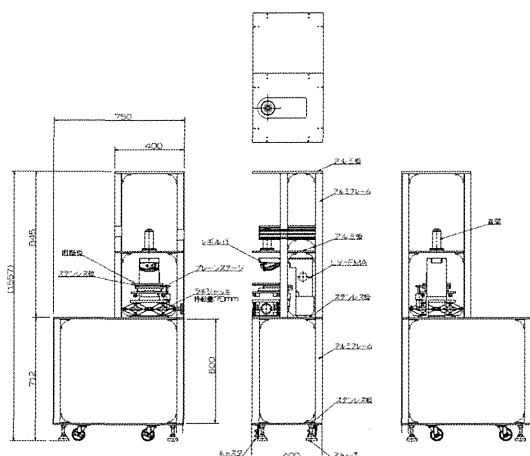

図 1　ブタ用顕微鏡システム図（俯瞰）

図2　ブタ観察システム三面図

(2) マウスレベルでの予備検討

　動脈硬化のように血管が主な傷害の場になる病態だけでなく、血栓症、腫瘍やメタボリックシンドロームにおいても、血流や血管機能といった生体内のダイナミックな変化、組織学的変化に先行する初期の炎症性変化を捉えることが可能な生体内分子イメージング技術は非常に有用である。従来の生体内観察では、透過光による観察が容易な腸間膜の微小循環を用いた研究が主に行なわれてきたが、近年の光学観察系・蛍光プローブの開発により、蛍光物質をトレーサーとして、透過光観察が不可能な厚みを有する脂肪組織をはじめとする実質臓器の血流観察も可能となった。時間・空間解像度も飛躍的に改善し、細胞内小器官レベルでの解析が可能となっている。

　そこで、我々は蛍光プローブと遺伝子改変動物を組み合わせて、マルチカラー高速イメージングを行った。さらに、マウスにおいて活性酸素産生を光化学反応にて誘導する系を確立し、血栓形成を観察した。

　さらにヒト iPS 細胞由来人工血小板を作製し、機能評価を行った。通常のマウスでは、ヒト iPS 細胞由来人工血小板は輸血しても網内系に Trap されてしまうが、免疫不全(NOG マウス)を用いることで回避した。

(3) 倫理面への配慮

　本研究では動物実験が含まれる。動物愛護には最大限の配慮を払う。動物実験プロトコールは、「研究機関等における動物実験等の実施に関する基本指針」に従い、以下のとおり機関内承認を得た。

・マウス実験

　西村智申請「血栓形成メカニズムの病態解明」

　平成 25 年 11 月 8 日承認

　承認番号　第 13243 号

　変更申請　平成 26 年 1 月 29 日承認

　承認番号　第 13243 号

・ブタ実験

　西村智申請「ブタを用いたバイオイメージングの初期検討」

　平成 26 年 4 月 18 日承認

　承認番号　第 14227 号

　なお、本学ピッグセンターは、「Association for Assessment and Accreditation of Laboratory Animal Care International(国際実験動物管理公認協会、AAALAC)」の認証を取得している。

　組換えDNA実験についても、以下のとおり機関内承認を得て実施した。

　西村智申請

　「血栓形成メカニズムの可視化」

　平成 25 年 9 月 26 日承認

　許可番号　13−111

　改定版　平成 26 年 3 月 13 日承認

　許可番号　13−138

C. 研究結果

(1) ブタ観察システムの開発

　ブタに適応可能なイメージングシステムを開発し、Dry Lab で結像を確認した。ただし、

ブタに応用するためには、
・Two Camera に適応したソフトウェア制御（NISE elements を使用予定）
・CSU X1 と Two Camera の光軸調整
・マイクロミニブタのハンドリング（麻酔・色素投与経路）
など細かい技術的問題がある。これらは、それぞれ、要素技術を開発しており、短期間で解決すると思われる。

(2) マウスレベルでの予備検討

　マウスでは、一光子・二光子顕微鏡を用いて下記の図のように多くの組織において画像取得が可能になった（図3−5）。時間・空間解像度も飛躍的に改善し、細胞内小器官レベルでの解析が可能となっている（Nishimura et al, 2008 JCI; Nishimura et al, 2012 Blood; Nishimura et al, 2010 JCI; Nishimura et al, 2012 Cell Metabolism; Nishimura et al, 2009 Nature Medicine)。
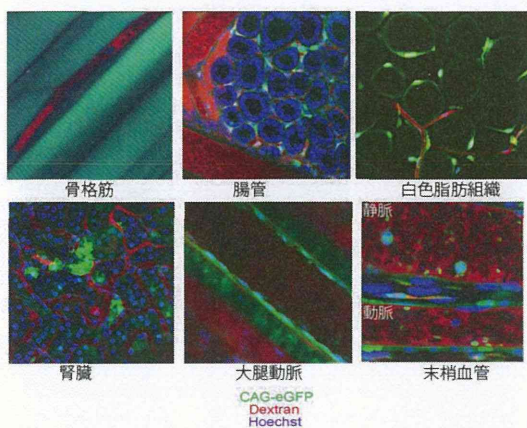

図3　「生体イメージング」でみる代謝組織・血管
「生体イメージング」では手に取るように末梢臓器や血管における生体内の各種細胞の動きが分かる。CAG-eGFP マウスに、Texas Red Dextran と Hoechst を投与している。

図4　「生体イメージング」でみる末梢血管
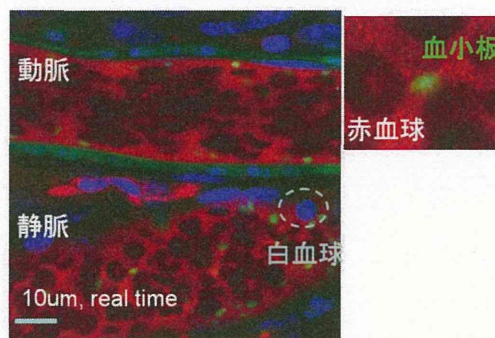「生体イメージング」では動脈・静脈において、血小板・赤血球・白血球を同定し、動的に観察が可能になった。CAG-eGFP マウスに、Texas Red Dextran と Hoechst を投与している。

　我々は、レーザー傷害による ROS 産生を伴う血栓形成モデルと、上記の生体イメージングを組み合わせ、血小板機能に異常を来す各種遺伝子改変動物における血栓形成過程を観察し、生体内での血小板機能との関係を明らかにした。図5のように、ROS 刺激により高い再現性をもって、血管内に血栓を誘導することに成功した。
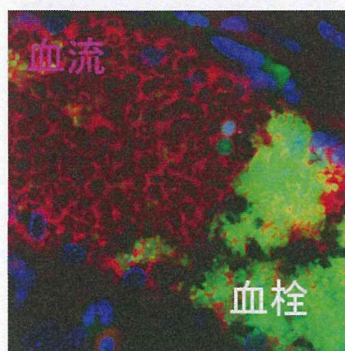

図5　生体内血栓イメージ
緑：血小板　赤：血流　レーザー照射により誘発された微小血栓の形成過程。生体イメージングとレーザー傷害を組み合わせることにより、腸間膜の毛細血管において、血栓を誘発し、血栓形成に寄与する単一血小板を可視化することが可能になった。レーザー照射により血小板血栓が発達している。

（3）ヒト iPS 細胞由来人工血小板の生体内機能解析

近年の多能性幹細胞（ES，iPS）の研究の進歩により、細胞療法を含む再生医学での広い範囲での臨床応用が期待されている。しかし、これらの幹細胞を用いた基礎研究を臨床現場に繋げるためには、in vitro での知見を、ヒトを対象とした研究に応用する前に、実際に試験管内で作製した細胞が、実際の個体（マウスおよび大動物）の中でどのように機能しているか、どのように病変に働くかを明らかにすることは必須である。我々は、京都大学 iPS 細胞研究所江藤教授チームとの共同研究の結果、iPS 細胞を誘導するのに必要な山中四因子の中の c-Myc の発現をコントロールすることにより、飛躍的かつ効率的に、ヒト iPS 由来の人工血小板を作製する手法を確立した。我々は生体イメージングを用いて、こうして得られたヒト iPS 由来血小板の体内動態の可視化を行った。観察に用いた免疫不全マウス（NOG マウス）の体内では、iPS 由来人工血小板の細胞動態が捉えられた（図6）。iPS 由来血小板がマウス体内を循環しているだけでなく、レーザー傷害により誘発された血栓形成部位においてはホスト血小板と iPS 由来血小板が相互作用しながら血栓を形成するさまが観察された。つまり、「人工血小板は体内を循環し、血栓も作る」ことが証明されたわけである。このように、本イメージ手法は iPS 分化誘導細胞を用いた細胞療法の臨床応用に向けて、安全性・有用性を評価する上できわめて有用性が高い手法と言える。さらに、最近では、人工血小板の作製を飛躍的に効率的にする手法を開発した（Takayama, Nishimura et al, 2012 JEM; Nakamura, Nishimura, Eto, et al, 2014 Cell Stem Cell）。
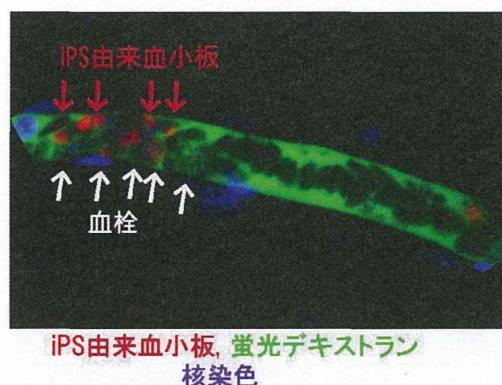
図 6 生体内における iPS 由来人工血小板の血栓形成過程

レーザー照射により誘発された iPS 由来人工血小板の血栓形成過程。20 秒のレーザー照射により人工血小板を含む血小板血栓が発達し血管径が狭小化している。

D. 考察

生体の各種病態下での細胞連関・情報伝達異常をより明らかにするためには、形態と機能とを組み合わせた光イメージングが今後必要になると考えられる。

ブタレベルでの光イメージングを立ち上げることで、今後は、再生医療や創薬のプロセスを飛躍的に加速すると思われた。

但し、大型動物故の技術的問題も多く、ブタでのイメージングを進めるには、光学機器メーカー企業とも密に連携をとりながら技術開発を進める必要があると考えられる。

E. 結論

ブタレベルでの光イメージングは技術的困難を伴うものの、他の手法にくらべて圧倒的に時間・空間解像度が高いことからも、きわめて強いインパクトが期待できる。マウスレベルでの基礎技術を集約しつつ、機器メーカーとも協働しながら、一光子、将来的には、二光子イメージングを立ち上げることは必須

の展開だと考えられた。

F. 健康危険情報

（分担研究報告書には記入せずに、総括研究報告書にまとめて記入した。）

G. 研究発表

論文発表

1. Nakamura, S., Takayama, N., Hirata, S., Seo, H., Endo, H., Ochi, K., Fujita, K.-I., Koike, T., Harimoto, K.-I., Dohda, T., Watanabe, A., Okita, K., Takahashi, N., Sawaguchi, A., Yamanaka, S., Nakauchi, H., **Nishimura, S.**, Eto, K.: Expandable megakaryocyte cell lines enable clinically applicable generation of platelets from human induced pluripotent stem cells. *Cell Stem Cell* 2014 Apr. 3; 14(4): 535–548. (doi: 10.1016/j.stem.2014.01.011.) Epub 2014 Feb. 13.

2. Kunishima, S., **Nishimura, S.**, Suzuki, H., Imaizumi, M., Saito, H.: TUBB1 mutation disrupting microtubule assembly impairs proplatelet formation and results in congenital macrothrombocytopenia. *European Journal of Haematology* 2014 Apr.; 92(4): 276–282. (doi: 10.1111/ejh.12252.) Epub 2014 Jan. 11.

3. Sakata, A., Ohmori, T., **Nishimura, S.**, Suzuki, H., Madoiwa, S., Mimuro, J., Kario, K., Sakata, Y.: Paxillin is an intrinsic negative regulator of platelet activation in mice. *Thrombosis Journal* 2014 Jan. 2; 12(1): 1. (doi: 10.1186/1477-9560-12-1.)

4. 西村智: 生体分子イメージングによる血栓形成・血管機能の可視化. *日本血栓止血学会誌* 2013; 24(6): 588–592.

5. **Nishimura, S.**, Manabe, I., Takaki, S., Nagaskai, M., Ostu, M., Yamashita, H., Sugita, J., Yoshimura, K., Eto, K., Komuro, I., Kadowaki, T., Nagai, R.: Adipose natural regulatory B cells negatively control adipose tissue inflammation. *Cell Metabolism* 2013 Nov. 5; 18: 759–766.

6. 西村智: 生体分子イメージングによる血栓の可視化. *日本血栓止血学会誌* 2013; 24(4): 396–401.

7. 西村智: 生体二光子イメージングによる生活習慣病の分子機構を慢性炎症の寄与. *日本レーザー医学会誌* 2013; 34(2): 77–81.

学会発表

1. 西村智: 血栓形成の生体内分子イメージングによる可視化：血管内皮傷害の関与. 第14回 TTMフォーラム, 東京, 2014年3月8日.

2. 西村智: 生体非線形分子イメージング
による生活習慣病病態解析. 第8回
有機分子バイオエレクトロニクス分科会,
東京, 2014年3月5日.

3. Nishimura, S.: Conceptualize,
construct, integrate and
understand life. TSBMI 第7回シン
ポジウム, 東京, 2014年2月28日.

4. 西村智: 新規光生体イメージングによ
る慢性炎症を基盤とする生活習慣病病
態の解明. NEXT シンポジウム, 東京,
2014年2月28日.

5. 西村智: 蛍光で生体を見る. 宮崎サイ
エンスキャンプ, 宮崎, 2014年2月
14–16日.

6. 西村智: 生体分子イメージングで明ら
かになる肥満脂肪組織における免疫・
炎症性細胞の賦活化機構. 第28回日
本糖尿病・肥満動物学会年次学術集
会, 宮崎, 2014年2月14–15日.

7. Nishimura, S.: Artery cell
contractions via ROS and NO
balance visualized by in vivo
multiphoton imaging technique.
23rd Australian Conference on
microscopy and microanalysis
(ACMM23), Adelaide, Australia,
February 2–6, 2014.

8. Nishimura, S.: Thrombus
development processes are
dependent on endothelial injuries:
examined by in vivo molecular
imaging. 23rd Australian
Conference on microscopy and

microanalysis (ACMM23),
Adelaide, Australia, February 2–6,
2014.

9. 西村智: レーザー障害に伴う平滑筋収
縮と血栓形成: 生体二光子分子イメー
ジングによる可視化. レーザー学会第
33回年次大会, 北九州, 2014年1月
20–22日.

10. 西村智: 光でみる生活習慣病と慢性
炎症. 第1回メタボリックネットワーク研
究会, 福岡, 2014年1月18日.

11. Nishimura, S.: In vivo
multi-photon molecular imaging
technique reveals immune and
inflammatory cell cross-talks and
activation processes in metabolic
diseases. 第42回日本免疫学会学術
集会, 千葉, 2013年12月11–13日.

12. 西村智: 生活習慣病における免疫・炎
症性細胞クロストークの二光子イメージ
ングによる可視化. 第36回日本分子
生物学会年会, 神戸, 2013年12月
3–6日.

13. Nishimura, S.: In vivo
multi-photon molecular imaging
reveals immune cell cross-talks
and activation processes in
metabolic diseases and obesity.
The 3rd CSI/JSI/KAI Joint
Symposium, Korea, December 1–3,
2013.

14. 西村智: 生活習慣病における免疫・炎
症性細胞クロストークの可視化. 第41

回日本臨床免疫学会総会，下関，2013 年 11 月 28 日．

15. 西村智: 生体分子イメージングでみる活性酸素刺激による血管平滑筋収縮機構の解明．第 17 回日本心血管内分泌代謝学会学術総会，大阪，2013 年 11 月 22–23 日．

16. 西村智: 生体分子イメージングでみる肥満脂肪組織における免疫・炎症細胞のクロストーク．第 17 回日本心血管内分泌代謝学会学術総会，大阪，2013 年 11 月 22–23 日．

17. 西村智: 蛍光イメージでみる生活習慣病における生体破綻メカニズム．第 29 回 Wako ワークショップ「蛍光生体イメージング：見ることによって切り拓く新しい研究展開」，東京，2013 年 11 月 4–6 日．

18. 西村智: 生体イメージングの基礎と応用．第 6 回麻酔科痛みのメカニズムを語る会，東京，2013 年 10 月 26 日．

19. 西村智: 生体分子イメージングでみる肥満病態における免疫・炎症性細胞のクロストーク．第 34 回日本肥満学会，東京，2013 年 10 月 12–13 日．

20. Nishimura, S., Eto, K., Nagai, R.: Thrombus formation with discoid platelet aggregations visualized by in vivo molecular imaging technique in mice. 第 75 回日本血液学会学術集会，札幌，2013 年 10 月 11–13 日．

21. Nishimura, S., Eto, K., Nagai, R.: In vivo imaging visualize thrombopoiesis and elucidate the programming humoral factors. 第 75 回日本血液学会学術集会，札幌，2013 年 10 月 11–13 日．

22. Nishimura, S., Eto, K., Nagai, R.: Thrombus formation with discoid platelet aggregations visualized by in vivo molecular imaging methods in mice. 2013 Eurothrombosis, Sweden, October 3–5, 2013.

23. 西村智, 長崎実佳: 生体分子イメージングでみる生活習慣病における免疫・炎症性細胞のクロストーク．第 45 回日本臨床分子形態学会，福岡，2013 年 9 月 13–14 日．

24. 西村智, 永井良三: 生体二光子イメージングでみる肥満脂肪組織における免疫・炎症性細胞のクロストーク．第 4 回 Molecular Cardiovascular Conference II, キロロ，2013 年 9 月 6–8 日．

25. 西村智, 長崎実佳: 肥満・動脈硬化は初期記銘力・高次機能低下を規定する．第 54 回日本人間ドック学会学術大会，浜松，2013 年 8 月 29–30 日．

26. 長崎実佳, 西村智: メタボリックシンドロームを規定する血清修飾リン脂質．第 54 回日本人間ドック学会学術大会，浜松，2013 年 8 月 29–30 日．

27. Nishimura, S.: Seeing the cells and molecules in living animals.

Asahct 2013, 仙台, 2013 年 8 月
27–28 日.

28. <u>Nishimura, S.</u>: Immune and inflammatory cell cross-talks and activation processes in metabolic diseases. 11th Japan-Korea Joint Symposium on Vascular Biology, Jeju, Korea, August 22–24, 2013.

29. <u>西村智</u>, 長崎実佳: 生体イメージングでみる平滑収縮筋と血液内皮障害. 第 55 回日本平滑筋学会総会, 旭川, 2013 年 8 月 7–8 日.

30. <u>Nishimura, S.</u>: Autotaxin contribute to the adipose tissue expansion and inflammation in diet-induced-obesity in mice. FASEB meeting, ニセコ, 2013 年 8 月 4–9 日.

31. <u>西村智</u>: 生体分子イメージングでみる生活習慣病態における免疫・炎症性細胞のクロストーク. 第 23 回日本病態生理学会, 東京, 2013 年 8 月 2–3 日.

32. <u>西村智</u>, 長崎実佳: 生体二光子イメージングで明らかになる肥満脂肪組織における免疫・炎症性細胞のクロストーク. 第 45 回日本動脈硬化学会総会, 新宿, 2013 年 7 月 18–19 日.

33. <u>西村智</u>, 長崎実佳: 生体分子イメージングでみる平滑収縮筋と血管内皮障害. 第 45 回日本動脈硬化学会総会, 新宿, 2013 年 7 月 18–19 日.

34. <u>西村智</u>: 生体分子イメージングによる炎症を基盤とする生活習慣病へのアプ

ローチ. 第 8 回神戸生活習慣病研究会, 神戸, 2013 年 7 月 13 日.

35. <u>西村智</u>, 永井良三: 生体分子イメージングでみる生活習慣病における免疫・炎症細胞のクロストーク. TMFC, 大阪, 2013 年 7 月 6–7 日.

36. <u>西村智</u>: 生体分子イメージングでみる活性酸素と NO バランスによる平滑筋収縮過程. 第 13 回日本 NO 学会学術集会, 那覇, 2013 年 6 月 28–29 日.

37. <u>西村智</u>: フローサイトメトリーによる生体解析の進歩. 第 23 回日本サイトメトリー学会学術集会 シンポジウム「イメージング技術の進歩と医学への応用」, 東京, 2013 年 6 月 22–23 日.

38. <u>西村智</u>, 長崎実佳: 生活習慣病における免疫・炎症性細胞のクロストーク. 第 23 回日本サイトメトリー学会学術集会 シンポジウム「再生と炎症、新たな展望」, 東京, 2013 年 6 月 22–23 日.

39. <u>西村智</u>: 血栓形成のメカニズム. 第 23 回日本サイトメトリー学会学術集会, 東京, 2013 年 6 月 22–23 日.

40. <u>西村智</u>, 長崎実佳, 真鍋一郎, 中村和宏, 大川龍之介, 奥平真一, 青木淳賢, 矢冨裕, 小室一成, 永井良三: 血清リン脂質・生合成系を標的とした新規メタボリックシンドロームマーカーの探索, 第 55 回日本脂質生化学会, 仙台, 2013 年 6 月 6–7 日.

41. <u>Nishimura, S.</u>, Nagasaki, M., Nagai, R.: - Novel approaches to

platelet functions in vivo ‐ Discoid platelet aggregations and biogenesis of platelet visualized by in vivo molecular imaging. 第 35 回日本血栓止血学会学術集会　SPC シンポジウム.血小板生理機能への多面的アプローチ, 山形, 2013 年 5 月 30 日–6 月 1 日.

42. <u>Nishimura, S.</u>: Platelet aggregations and thrombopoiesis visualized by in vivo molecular imaging. 第 35 回日本血栓止血学会学術集会, 山形, 2013 年 5 月 30 日–6 月 1 日.

43. <u>西村智</u>: 生体分子イメージングでみる血栓形成メカニズム. 第 35 回日本血栓止血学会学術集会, 山形, 2013 年 5 月 30 日–6 月 1 日.

44. <u>西村智</u>: 生体分子イメージングでみる炎症および血栓形成メカニズム. 第 69 回日本顕微鏡学会学術講演会　シンポジウム「最新の光学イメージングと生体観察」, 大阪, 2013 年 5 月 20–22 日.

45. <u>西村智</u>: 生体二光子分子イメージングでみる肥満脂肪組織における免疫・炎症細胞のクロストーク. 第 69 回日本顕微鏡学会学術講演会, 大阪, 2013 年 5 月 20–22 日.

46. <u>西村智</u>, 長崎実佳, 真鍋一郎, 江藤浩之, 小室一成, 永井良三: 生体二光子イメージングでみる肥満脂肪組織にお

ける免疫・炎症性細胞のクロストーク. 第 56 回日本糖尿病学会年次学術集会, 熊本, 2013 年 5 月 16–18 日.

47. <u>Nishimura, S.</u>, Nagasaki, M.: In vivo multi-photon molecular imaging technique visualizes immune and inflammatory cell cross-talks in metabolic diseases. Immunology 2013, Honolulu, May 3–7, 2013.

48. <u>西村智</u>: 生体分子イメージングによる生活習慣病へのアプローチ. 第 86 回日本内分泌学会学術総会　若手研究者シンポジウム, 仙台, 2013 年 4 月 25–26 日.

49. <u>西村智</u>, 長崎実佳: 生体分子イメージングでみる生活習慣病における免疫・炎症性細胞のクロストーク. 第 50 回臨床分子医学会, 東京, 2013 年 4 月 12–13 日.

H. 知的財産権の出願・登録状況

特許
発明者:<u>西村智</u>
発明の名称:生体イメージングによる血小板機能評価システム
出願日:平成 22 年 6 月 1 日
出願番号:特願 2010–125869

研究成果の刊行に関する一覧表

書籍

著者氏名	論文タイトル名	書籍全体の編集者名	書 籍 名	出版社名	出版地	出版年	ページ

雑誌

発表者氏名	論文タイトル名	発表誌名	巻号	ページ	出版年
Nakamura, S., Takayama, N., Hirata, S., Seo, H., Endo, H., Ochi, K., Fujita, K.-I., Koike, T., Harimoto, K.-I., Dohda, T., Watanabe, A., Okita, K., Takahashi, N., Sawaguchi, A., Yamanaka, S., Nakauchi, H., **Nishimura, S.**, Eto, K.	Expandable megakaryocyte cell lines enable clinically applicable generation of platelets from human induced pluripotent stem cells	Cell Stem Cell	14(4)	535–548	2014
Kunishima, S., **Nishimura, S.**, Suzuki, H., Imaizumi, M., Saito, H.	TUBB1 mutation disrupting microtubule assembly impairs proplatelet formation and results in congenital macrothrombocytopenia	European Journal of Haematology	92(4)	276–282	2014
Sakata, A., Ohmori, T., **Nishimura, S.**, Suzuki, H., Madoiwa, S., Mimuro, J., Kario, K., Sakata, Y.	Paxillin is an intrinsic negative regulator of platelet activation in mice	Thrombosis Journal	12(1)	1	2014

発表者氏名	論文タイトル名	発表誌名	巻号	ページ	出版年
西村智	生体分子イメージングによる血栓形成・血管機能の可視化	日本血栓止血学会誌	24(6)	588–592	2013
Nishimura, S., Manabe, I., Takaki, S., Nagaskai, M., Ostu, M., Yamahsita, H., Sugita, J., Yoshimura, K., Eto, K., Komuro, I., Kadowaki, T., Nagai, R.	Adipose natural regulatory B cells negatively control adipose tissue inflammation	Cell Metabolism	18	759–766	2013
Watanabe, M., Nakano, K., Matsunari, H., Matsuda, T., Maehara, M., Kanai, T., Kobayashi, M., Matsumura, Y., Sakai, R., Kuramoto, M., Hayashida, G., Asano, Y., Takayanagi, S., Arai, Y., Umeyama, K., Nagaya, M., Hanazono, Y., Nagashima, H.	Generation of interleukin-2 receptor gamma gene knockout pigs from somatic cells genetically modified by zinc finger nuclease-encoding mRNA	PLOS ONE	8(10)	e76478	2013
西村智	生体分子イメージングによる血栓の可視化	日本血栓止血学会誌	24(4)	396–401	2013
Arai, Y., Ohgane, J., Fujishiro, S.-H., Nakano, K., Matsunari, H., Watanabe, M., Umeyama, K., Azuma, D., Uchida, N., Sakamoto, N., Makino, T., Yagi, S., Shiota, K., Hanazono, Y., Nagashima, H.	DNA methylation profiles provide a viable index for porcine pluripotent stem cells	Genesis	51	763–776	2013

発表者氏名	論文タイトル名	発表誌名	巻号	ページ	出版年
Klymiuk, N., Blutke, A., Graf, A., Krause, S., Burkhardt, K., Wuensch, A., Krebs, S., Kessler, B., Zakhartchenko, V., Kurome, M., Kemter, E., **Nagashima, H.,** Schoser, B., Herbach, N., Blum, H., Wanke, R., Aartsma-Rus, A., Thirion, C., Lochmuller, H., Walter, M.C., Wolf, E.	Dystrophin-deficient pigs provide new insights into the hierarchy of physiological derangements of dystrophic muscle	Human Molecular Genetics	22(21)	4368–4382	2013
西村智	生体二光子イメージングによる生活習慣病の分子機構と慢性炎症の寄与	日本レーザー医学会誌	34(2)	77–81	2013
Nakano, K., Watanabe, M., Matsunari, H., Matsuda, T., Honda, K., Maehara, M., Kanai, T., Hayashida, G., Kobayashi, M., Kuramoto, M., Arai, Y., Umeyama, K., Fujishiro, S., Mizukami, Y., Nagaya, M., **Hanazono, Y., Nagashima, H.**	Generating porcine chimeras using inner cell mass cells and parthenogenetic preimplantation embryos	PLOS ONE	8(4)	e61900	2013
花園豊	大型動物を用いた幹細胞研究	臨床血液	54(4)	329–335	2013

研究成果の刊行物・別刷

Article

Expandable Megakaryocyte Cell Lines Enable Clinically Applicable Generation of Platelets from Human Induced Pluripotent Stem Cells

Sou Nakamura,[1] Naoya Takayama,[1] Shinji Hirata,[1] Hideya Seo,[1] Hiroshi Endo,[1] Kiyosumi Ochi,[1] Ken-ichi Fujita,[1] Tomo Koike,[1] Ken-ichi Harimoto,[1] Takeaki Dohda,[1] Akira Watanabe,[2] Keisuke Okita,[2] Nobuyasu Takahashi,[3] Akira Sawaguchi,[3] Shinya Yamanaka,[2] Hiromitsu Nakauchi,[4] Satoshi Nishimura,[5,6] and Koji Eto[1,4,*]

[1]Department of Clinical Application, Center for iPS Cell Research and Application (CiRA), Kyoto University, 606-8507, Japan
[2]Department of Reprogramming Science, CiRA, Kyoto University, 606-8507, Japan
[3]Department of Anatomy, Ultrastructural Cell Biology, Faculty of Medicine, University of Miyazaki, Miyazaki 889-1692, Japan
[4]Laboratory of Stem Cell Therapy, Center for Stem Cell Biology and Regenerative Medicine, Institute of Medical Science, The University of Tokyo, Tokyo 108-8639, Japan
[5]Department of Cardiovascular Medicine, The University of Tokyo, Tokyo 113-8655, Japan
[6]Department of Cell and Molecular Medicine, Center for Molecular Medicine, Jichi Medical University, Tochigi 329-0498, Japan
*Correspondence: kojieto@cira.kyoto-u.ac.jp
http://dx.doi.org/10.1016/j.stem.2014.01.011

SUMMARY

The donor-dependent supply of platelets is frequently insufficient to meet transfusion needs. To address this issue, we developed a clinically applicable strategy for the derivation of functional platelets from human pluripotent stem cells (PSCs). This approach involves the establishment of stable immortalized megakaryocyte progenitor cell lines (imMKCLs) from PSC-derived hematopoietic progenitors through the overexpression of BMI1 and BCL-XL to respectively suppress senescence and apoptosis and the constrained overexpression of c-MYC to promote proliferation. The resulting imMKCLs can be expanded in culture over extended periods (4–5 months), even after cryopreservation. Halting the overexpression of c-MYC, BMI1, and BCL-XL in growing imMKCLs led to the production of CD42b+ platelets with functionality comparable to that of native platelets on the basis of a range of assays in vitro and in vivo. The combination of robust expansion capacity and efficient platelet production means that appropriately selected imMKCL clones represent a potentially inexhaustible source of hPSC-derived platelets for clinical application.

INTRODUCTION

Platelets generated from megakaryocyte (MK) precursors are vital for the treatment of many hematological diseases and traumas. Currently, platelets can only be obtained through blood donation. Fresh single-donor platelets have a short shelf life and must be maintained with plasma at 20°C–24°C; they readily lose clotting activity when pooled from multiple donors and frozen or warmed to 37°C (Bergmeier et al., 2003; Nishikii et al., 2008). Moreover, repeated transfusion induces the production of anti-

bodies against allogenic human leukocyte antigen (HLA) or human platelet antigen (HPA) on the transfused platelets (Schiffer, 2001), which renders the patient unresponsive to platelet transfusion therapy. These supply logistics and practical limitations represent barriers to the widespread application of platelets as a resource for patients. In that context, human induced pluripotent stem cells (hiPSCs) (Takahashi et al., 2007) could represent a potent alternative source of platelet production. Because platelets do not contain nuclei, gamma irradiation before transfusion could be used to eliminate any residual contaminating hiPSCs and their derivatives, reducing the risk of tumorigenesis. Thus, the application of iPSC-based technology could potentially yield a consistent supply of HLA- and/or HPA-matched or even autologous platelets in a way that would address some of the major roadblocks in the current clinical approaches to platelet-based therapy.

Our group and another recently demonstrated that hiPSCs derived from human skin fibroblasts or blood cells or from human embryonic stem cells (hESCs) can be used to generate platelets in vitro and that these platelets appeared to function normally when transfused into mouse models (Takayama et al., 2010; Lu et al., 2011). However, the yield of platelets was still far below what would be required to generate even 1 u of platelet concentrate for patient transfusion. Recent studies have shown that self-replicating MK progenitors can be directly generated from murine hematopoietic stem cells (HSCs) within bone marrow (BM) in vivo (Yamamoto et al., 2013), but there was no evident way to sustain long-term self-replication of MK progenitors in vitro. We previously showed that the activation of c-MYC to a restricted level below that associated with senescence and apoptosis induction appears to lead to an increase in platelet generation (Takayama et al., 2010). In the present study, we show that co-overexpression of c-MYC and BMI1, a polycomb complex component that represses the *INK4A/ARF* gene locus (Oguro et al., 2006), enables megakaryocytic cell lines (MKCLs) derived from hiPSCs or hESCs to grow continuously for up to 2 months. A destabilization domain (DD) vector system (Banaszynski et al., 2006) enabled us to control exogenous c-MYC within the appropriate range, leading to successful induction of
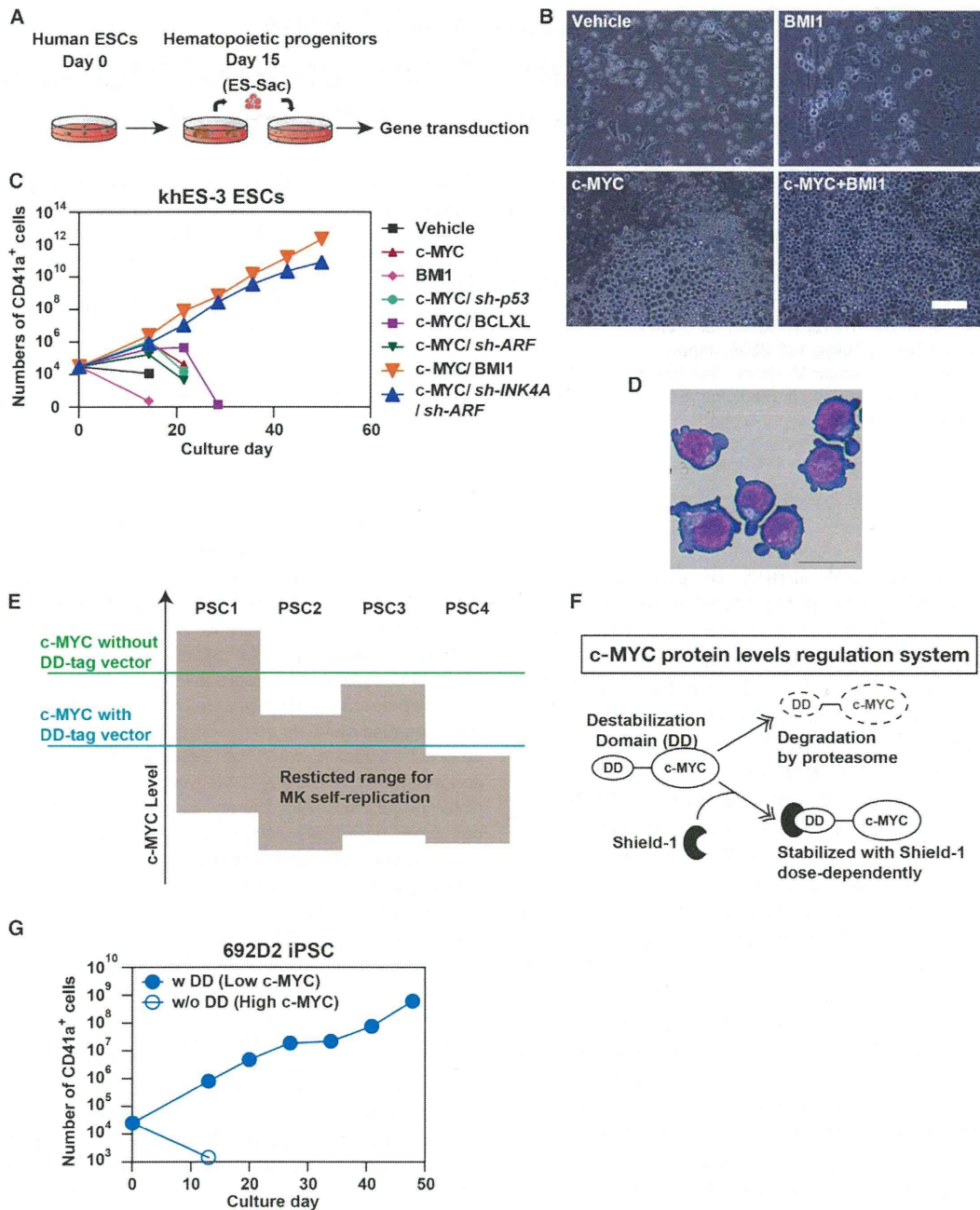
Figure 1. Induction of a Megakaryocyte Progenitor Cell Line from Human Embryonic Stem Cells and Induced Pluripotent Stem Cells Was Induced by Restricted Range of c-MYC Overexpression along with BMI1 Overexpression

(A) Scheme for inducing megakaryocyte progenitor cell lines (MKCLs) from human PSCs. The targets for gene transduction are hematopoietic progenitors, including the CD34^{+} population.

(B) Representative photomicrograph of cells transduced with vector alone, c-MYC alone, BMI1 alone, or a combination of c-MYC and BMI1 (200×). The scale bar represents 100 μm.

(C) Numbers of CD41a^{+} cells after gene manipulation. Hematopoietic progenitor cells (HPCs) within human embryonic stem cell (hESC; KhES-3 clone) sacs were collected and transduced with noninducible retroviral vectors with vector alone (GFP alone), c-MYC alone, BMI1 alone, or combinations of c-MYC plus *p53* knockdown, c-MYC plus *ARF* knockdown, c-MYC plus BCL-XL, c-MYC plus *INK4A/ARF* knockdown (blue), or c-MYC plus BMI1 (orange). The combinations of c-MYC plus BMI1 and c-MYC plus *INK4A/ARF* knockdown induced exponential growth in CD41a^{+} megakaryocytes (MKs). Results are expressed as means from two to three independent experiments.

(D) Representative image of May-Giemsa-stained MKCLs. The scale bar represents 20 μm.

(legend continued on next page)

MKCLs. The addition of BCL-XL made it possible to obtain immortalized MKCLs (imMKCLs) that can be grown for more than 5 months and thus function as candidate cell banks. When the expression of c-MYC, BMI1, and BCL-XL is turned off, imMKCLs produce functional CD42b (glycoprotein Ib α [GPIbα] and receptor for von Willebrand factor [vWF])[+] platelet particles. The expression of CD42b on platelets is required for the initiation of clotting (Ware et al., 2000) and bacterial clearance in vivo (Wong et al., 2013). Although previous studies have reported that CMK, Meg01, and K562 cells, three well-known MK lineage leukemia cell lines, can become polyploid and release CD41a^{+} particles in the presence of agonist stimulation, they do not provide a suitable source for a platelet supply because the particles are CD42b^{−} (Isakari et al., 2009; Sato et al., 1989; Terui et al., 1998). In this report, we describe a strategy that involves MKCLs with long-term self-renewal capacity and the potential to provide an inexhaustible supply of CD42b^{+} platelets; in that respect, they resemble endogenous self-replicating MK progenitors identified in vivo (Yamamoto et al., 2013). Clinical application of this technology could provide a plentiful supply of platelets from suitably screened and selected imMKCL clones to serve as cell bank stocks with minimal risk of adverse side effects.

RESULTS

Induction of Expandable MK Progenitor Cells from Human PSCs with c-MYC and BMI1

We previously showed that, when expressed at an appropriate level, c-MYC acts as a growth mediator in normal megakaryopoiesis and thrombopoiesis from hESCs or hiPSCs, whereas excessive c-MYC expression in hematopoietic progenitor cells (HPCs) induces the activation of the INK4A and ARF pathways, leading to senescence and apoptosis (Takayama et al., 2010). Therefore, we hypothesized that c-MYC activation might contribute to self-replication at the MK progenitor stage. When we assessed the effects of c-MYC overexpression alone, BMI1 overexpression alone, c-MYC overexpression plus p53 knockdown, c-MYC plus BCL-XL overexpression, and c-MYC plus BMI1 overexpression in CD34^{+}CD43^{+}-containing HPCs derived from the KhES-3 hESC line, we found that c-MYC overexpression alone or the combination of c-MYC and BMI1 overexpression increased numbers of large cells expressing megakaryocytic CD41a^{+}CD42a (GPIX)[+]CD42b^{+}CD9^{+} markers over a 2-week period (Figures 1A–1C; Figure S1A available online). With c-MYC and BMI1 overexpression (Figure 1C, orange triangles) or c-MYC overexpression and INK4A/ARF knockdown (Figure 1C, blue triangles), but none of the other aforementioned conditions, proliferation of this cell population was maintained at an exponential level for 2 months (MK progenitor cell line; Figure 1C, orange triangles) and was dependent upon the presence of thrombopoietin (TPO) with the help of

stem cell factor (SCF). This suggests that the effect of BMI1 may be to at least inhibit INK4A/ARF-dependent senescence and apoptosis during the initiation of self-replication, as confirmed by quantitative PCR (qPCR) analysis, which revealed BMI1 represses c-MYC-induced the upregulation of INK4A/ARF (Figure S1B). The CD41a^{+} MKCLs derived from hESCs showed monoblastic morphology with basophilic cytoplasm (Figure 1D) and generated aberrant platelet-like particles expressing normal levels of CD41a but reduced levels of CD42b (Figure S1C). This is consistent with the requirement for the downregulation of c-MYC for maturation of MKs (Takayama et al., 2010).

A Defined c-MYC Expression Level Is Important for MKCL Induction and Robust Expansion

Our ability to induce MKCLs with c-MYC and BMI1 overexpression and then grow the cells for more than 2 weeks varied among individual PSC clones (data not shown). Therefore, we suspected that individual PSC clones require different levels of c-MYC. When we prepared an inducible all-in-one vector harboring c-MYC and BMI1 (Ohmine et al., 2001) (Figure S1D), we obtained clearer evidence that c-MYC levels are crucial for the sustained growth of MKCL, given that we saw different results with c-MYC-2A-BMI1 and BMI1-2A-c-MYC gene sequences in this vector (Figures S1E and S1F). Furthermore, to confirm the hypothesis that, in some individual PSC clones, the effective c-MYC expression level may be restricted to a specific range (Figure 1E), we used a vector tagged with a DD (Banaszynski et al., 2006) in order to reduce the level of c-MYC protein (Figure 1F). This system regulates protein stability, and thus the level of c-MYC expression, in a manner that depends on the Shield1 concentration (NIH 3T3 cells in Figure S1G). When we used this DD-tagged vector system to establish iPSC (692D2)-derived MKCLs, we found that 692D2 iPSCs showed no self-replication when transduced with c-MYC-2A-BMI1 overexpression without a DD tag, but transduction of the DD tag vector without the addition of Shield1 allowed clone 692D2 to grow for up to 50 days in culture (Figure 1G). This self-replication was inhibited by 100 or 1,000 nM Shield1 (Figure 2Ai), suggesting the total c-MYC level most likely blocked stable self-replication. This result was not due to nonspecific cell toxicity (Figure S2A) or activation of the INK4A/ARF gene locus by the high level of c-MYC, given that levels of p14 and p16 mRNA (derived INK4A/ARF locus gene) did not differ in the presence or absence of 1,000 nM Shield1 (Figure S2B).

Given that BMI1, which is also overexpressed in our system, represses the INK4A/ARF gene locus, the mechanism underlying the MYC-dependent failure of continuous self-replication was unclear. However, the well-known involvement of c-MYC in caspase-dependent apoptosis (Juin et al., 2002) prompted us to assess caspase activity in the MKCL clone. Caspase assays revealed that the activation of caspases 3 and 7 in DD

(E) Schematic diagram illustrating the hypothesis that there is an association between c-MYC levels and MK self-replication. Individual human PSC clones (hESCs or hiPSCs) define the c-MYC activation window (restricted range) needed to induce MK self-replication.

(F) Scheme for a c-MYC regulation system using a destabilization domain (DD). Proteins with a DD are rapidly destroyed via the ubiquitin-proteasome pathway. Administration of Shield1 putatively inhibits DD-mediated degradation in a concentration-dependent manner.

(G) Numbers of CD41a^{+} MKs determined by flow cytometry. MKs were derived from iPSCs (692D2) transduced with inducible c-MYC-DD-2A-BMI1 (with [w] DD) or inducible c-MYC-2A-BMI1 retroviral vector (without [w/o] DD; see Figure S2A).
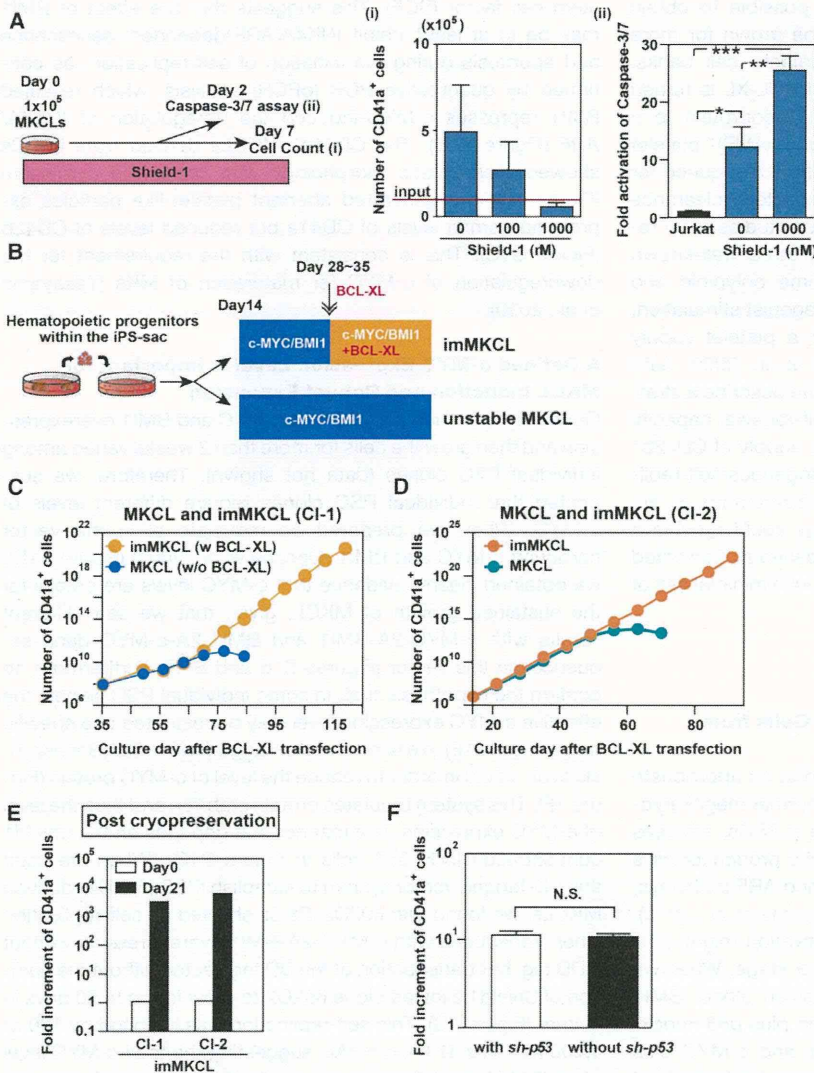
Figure 2. Later Expression of BCL-XL Inhibited Caspase Activation Induced by Excessive c-MYC, Stabilizing Cell Growth and Contributing to the Establishment of imMKCLs

(A) Relationship between the c-MYC expression level, cell viability, and caspase activity. (i) Numbers of live CD41a+ MKs derived from hiPSC (692D2)-based MKCLs generated with an inducible DD vector in the absence or presence of the indicated concentrations of Shield1. (ii) Caspase 3 and 7 activity in samples of Jurkat cells (control, fold = 1, black bar) or hiPSC (692D2)-derived MKCLs on day 2 of culture after transduction with a DD system in the absence or presence of 1,000 nM Shield1. *p < 0.05; **p < 0.01; ***p < 0.001. Results are expressed as means ± SE from five independent experiments.

(B) Scheme for generating unstable MKCLs with c-MYC and BMI1 (2F) or imMKCLs with c-MYC, BMI1, and BCL-XL (3F).

(C and D) Additional transduction of *BCL-XL* gene improved the growth curve for CD41a+ MKs derived from hiPSC (692D2)-derived MKCLs with a DD system (C; clone 1 [Cl-1]) and from hESCs (KhES3)-derived MKCLs (D; Cl-2). Yellow circles indicate the numbers of cells obtained with 3F, and blue circles indicate 2F. Cell numbers were calculated cumulative values.

(E) Increment in CD41a+ cells derived from Cl-1 and Cl-2 after cryopreservation. Results were an average of two independent experiments.

(F) The additional effect of *p53* knockdown on immortalization of MKCLs. Results are expressed as means ± SE from three independent experiments.

via mitochondrial outer membrane permeabilization. High levels of c-MYC also influenced cell-cycle-related genes, increasing the expression of cyclin-dependent kinase inhibitors (*CDKN1B*, *p27*, and *Kip1*), which could arrest MKCL growth. These changes were also confirmed by qPCR analysis (Figures S2C and S2D). Thus, high c-MYC expression can lead to caspase-dependent MKCL apoptosis (Figure 2A), despite the suppression of the INK4A/ARF pathway by BMI1 (Figure S2B). These data again indicate that alternative apoptosis pathways, as well as the INK4A/ARF pathways, are independently induced by excessive c-MYC in individual PSC-derived MKCL clones.

Suppression of Caspase Activation through BCL-XL Expression Promotes Immortalization

We noticed that MKCLs obtained from either ESC clone KhES3 or iPSC clone 692D2 with c-MYC plus BMI1 (Figure 2B, bottom line) exhibited limited growth potential and discontinuous cell growth that ceased at about 60 days, potentially reflecting an increase in caspase activation (692D2 cell growth in Figure 2C; KhES3 cell growth in Figure 2D; 0 nM Shield1 for 692D2 in Figure 2Ai and KhES-3 in Figure S2E). Thus, it appears that the expression of c-MYC and BMI1 alone are not suitable for

self-replicable MKCLs derived from iPSC clone 692D2 was 2-fold higher in the presence of 1,000 nM Shield1 than in its absence. This increased caspase activation was also associated with reduced cell viability (Figures 2Ai and 2Aii), confirming that restricting caspase activation may be key to successfully establishing expandable MKCLs (Figure S2B). Notably, caspase activation in the absence of Shield1 was still 12.2× higher than in Jurkat cells (Figure 2Aii). Some apoptotic events are transcriptionally determined (Chen et al., 2007; Kumar and Cakouros, 2004). Therefore, to further address the mechanism by which excessive c-MYC represses self-replication and induces apoptosis, we carried out a microarray analysis with iPSC-derived MKCLs treated with or without 1,000 nM Shield1. Gene ontology classification of genes differentially expressed in the presence and absence of Shield1 indicated a correlation between higher levels of c-MYC (1,000 nM Shield1) and the expression of the proapoptotic factors *BMF* and *BBC3* (*PUMA*), which can contribute to the release of cytochrome-c from mitochondria

generation of an immortalized cell line. We therefore sought to examine the effect of BCL-XL on days 14–21 after transduction of c-MYC plus BMI1 (Figure 2B). We found that BCL-XL overexpression induced exponential growth of CD41a$^+$ cells derived from either 692D2 or KhES3 cells. This growth persisted for over 5 months, and we therefore deemed these cells to be self-renewing imMKCLs (Figures 2C and 2D for 692D2 [imMKCL clone 1, Cl-1], and Figure 2D for KhES-3 ESCs [Cl-2]; yellow circles). These two imMKCLs also showed comparable growth after cryopreservation (Figure 2E) as well as somewhat larger cell size and expression of CD41a, CD42a, CD42b, and CD9 (Figure S2F). Growth of these imMKCLs was sustained even with higher c-MYC expression in the presence of 100 or 1,000 nM Shield1 (Figures S2G–S2I), and the cells exhibited comparatively low levels of caspase 3 and 7 activation, similar to that of Jurkat cells (Figure S2I).

To further validate the function of BCL-XL in caspase regulation, we tested the effect of the caspase inhibitor Z-VAD FMK on proliferation. Caspase inhibition increased proliferation about 21-fold, whereas BCL-XL expression elicited a 64-fold increase. In contrast, the vehicle control (DMSO) enhanced apoptosis (Figures S3A–S3C). Altogether, these findings again confirm that BCL-XL inhibits apoptosis through caspase 3 and 7 inactivation and that c-MYC, BMI1, and BCL-XL are all required for the induction of imMKCLs from PSC clones. In addition, because it is well known that activation of p53 and p21 is also associated with c-MYC-dependent apoptosis (Hotti et al., 2000), we assessed the effect of inhibiting p53 on cell growth with imMKCL Cl-1. Our results show no involvement of p53 in cells expressing c-MYC, BMI1, and BCL-XL (Figure 2F), and a similar result was obtained with KhES-3-imMKCL (Cl-2; data not shown).

Next, we asked whether the simultaneous overexpression of c-MYC, BMI1, and BCL-XL was more suitable for establishing imMKCLs than overexpression of c-MYC plus BMI1 followed by later expression of BCL-XL. To address that question, we used four individual PSC clones to compare two protocols: simultaneous overexpression of all three genes or overexpression of c-MYC and BMI1 followed by BCL-XL 14–21 days later, counting from the HPC stage (days 28–35 from the hESC or iPSC stage; Figure 2B, top). Simultaneous addition of all three genes promoted maximal proliferation for only up to 40–50 days, whereas stepwise addition of c-MYC and BMI1 followed by BCL-XL consistently showed more sustained proliferation with all clones examined (Figure S3D–S3G).

One potential caveat to this approach is that long-term cultivation might lead to imMKCLs becoming oncogenic. Interestingly, after cultivation for 5 months, two of three imMKCLs, Cl-1 and Cl-2 but not Cl-7, consistently showed a specific karyotypic abnormality: chromosomal translocation that included chromosome +1 or −5 (Figure S4A). When these two clones were separately infused into immunodeficient mice, one (n = 5) displayed leukemogenesis contributing to early death, but the other did not (Figure S4B). These results highlight the importance of transplantation studies with imMKCLs for clone selection. Interestingly, Cl-7 exhibited no karyotypic abnormality (Figure S4A) and consistently showed no abnormalities in transplantation studies (up to 16 weeks; Figure S4B). Therefore, we suggest that combined analysis, including both karyotypic examination and transplantation of individual imMKCL clones,

would be useful for selecting imMKCLs as cell bank stock candidates.

Differentiation Phase of imMKCLs for Upregulation of CD42b during Maturation

The GPIb-V-IX complex, particularly CD42b (GPIbα), on platelets is a key binding site for vWF and is required for the initial adhesion of platelets to an injured vessel wall (Ware et al., 2000) as well as normal circulation after transfusion (Leytin et al., 2004). Platelets lacking CD42b expression are quickly cleared from the circulation in vivo, leading to insufficient numbers of circulating platelets after transfusion (Nishikii et al., 2008). Assuming that the downregulation of c-MYC would be required for the generation of CD42b$^+$ platelets (Takayama et al., 2010), we turned off the expression of all three inducers (c-MYC, BMI1, and BCL-XL). Five days after these genes were turned off under serum-free conditions (Figure 3A), the iPSC-derived imMKCLs had changed to exhibit MK polyploidization (Figure 3B; on, 5.5% [left]; off, 20.2% [right]) as well as proplatelet formation (Figure 3C and Movie S1) with increased CD42b expression. This is exemplified by the two imMKCL clones in Figure 3D. Along with those changes, after turning off the expression of the exogenous inducing genes, both endogenous and exogenous c-MYC, BMI1, and BCL-XL expression declined (Figure S5A), and transcription factors associated with MK maturation, GATA1, FOG1, NFE2, and β1-tubulin increased to levels comparable to or higher than those seen in cord blood (CB)-derived MKs (Figure 3E).

Induction of Efficient Yield of CD41a$^+$CD42b$^+$ Platelets

Turning c-MYC, BMI1, and BCL-XL off with a doxycycline-regulated system increased the CD42b$^+$ platelet yield from imMKCLs and upregulated CD42b expression in CD41a$^+$ platelets (Figures 4A and 4B), in comparison to maintaining the overexpression of the three factors or BCL-XL alone (Figure S5B). In addition, whereas imMKCLs generated significant numbers of CD41a$^+$ CD42b$^+$ particles that closely resembled endogenous platelets, the well-known MKCLs Meg01, CMK, and K562, produced mostly CD41a$^+$, but CD42b$^-$, platelet-like particles (Figure S5C). We estimated production to be three CD42b$^+$ platelets per Cl-2 imMKCL-MK and 10 platelets per Cl-7 imMKCL-MK after the induction of differentiation (5 days after exogenous expression was turned off; Figure S5D) under serum-free conditions, which is a suitable level for clinical application. In a 10-cm dish scale (10 ml), 4×10^6 and 2×10^6 platelets per ml were obtained from imMKCL Cl-7 and Cl-2, respectively (Figure 4C). Therefore, our proposed system could theoretically yield 10^{11} platelets (equivalent to one transfusion) within 5 days with 25–50 l medium.

Characterization of platelet yields using flow cytometry revealed that the expression levels of platelet-functional molecules, including CD42b, CD61 (β3 integrin), protease-activated receptor 1 (PAR1; thrombin receptor), CD49b (α2 integrin), and CD29 (β1 integrin), were mostly comparable to those seen in fresh human peripheral blood (PB)-derived platelets and higher than in human endogenous pooled platelets, although the expression of GPVI (GP6) was a little weaker than it was in fresh PB (Figure 4D), possibly because of receptor shedding at 37°C (Gardiner et al., 2012). At the ultrastructural level, transmission
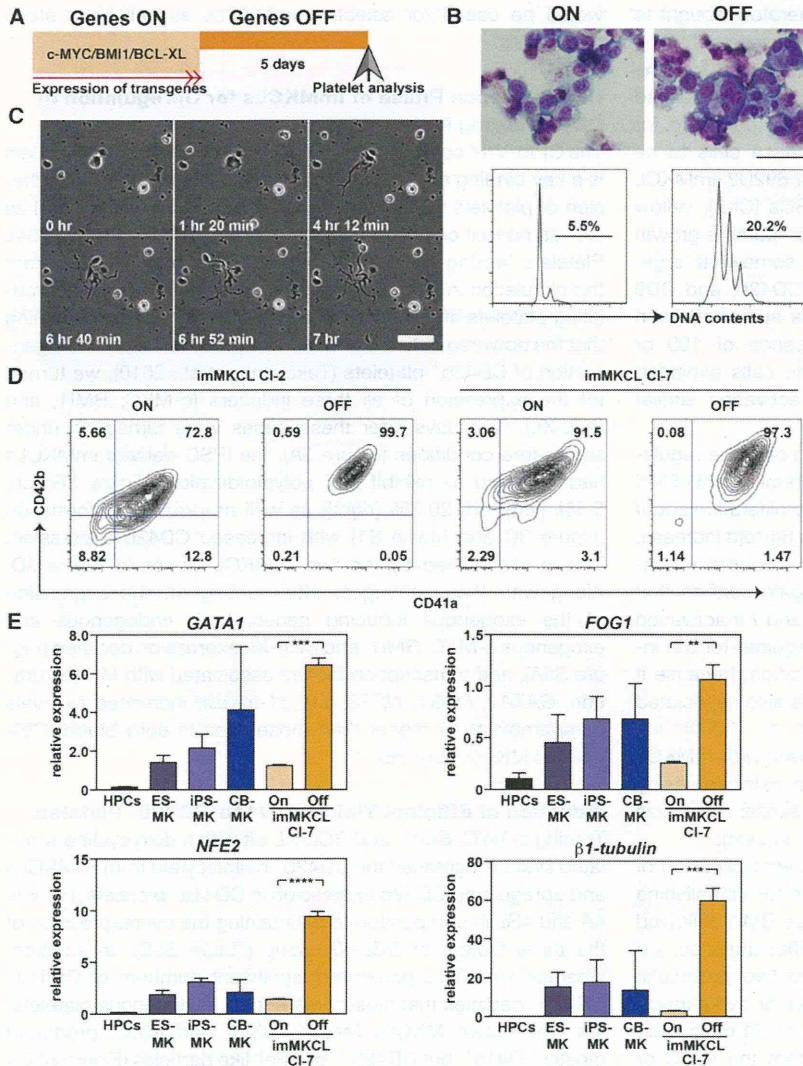
Figure 3. Turning Off 3F Transgenes Promoted the Maturation of MKs from imMKCLs

(A) MKs and platelets were analyzed 5 days after turning off 3F (cMYC, BMI1, and BCL-XL) expression.

(B) Giemsa staining (top pictures) and flow cytometric analysis of ploidy among imMKCLs with and without 3F expression (genes on or genes off). The scale bar represents 50 μm.

(C) imMKCL Cl-7 examined with time-lapse microscopy 4 days after genes were turned off. Sequential images showing proplatelet formation. The scale bar represents 50 μm.

(D) Representative contour plots for imMKCL Cl-2 and Cl-7 (MK populations are shown in side and forward scatter contour plots in a flow cytometer) derived from ESCs and iPSCs (KhES3 and DN-SeV2, respectively).

(E) qPCR analysis of GATA1, p45 NF-E2, FOG1, and β1-tubulin gene expression. Samples were obtained from hiPSC-derived CD34+/CD43+/CD41a−/GPA− HPCs (Sac-HPCs), Sac-dependent MKs from ESCs and iPSCs, MKs derived from cord blood (CB)-CD34+ cells, and imMKCL Cl-7 (DN-SeV2 iPSC clone) in the presence (on) or absence (off) of 3F. Gene expression was normalized to GAPDH expression. 3F was transduced into Sac-HPCs as described in the Experimental Procedures. Results are expressed as means ± SE from three independent experiments.

with a direct differentiation method (data not shown; Takayama et al., 2010) indicated their functionality was still sufficient to be useful. We also used an ex vivo flow chamber system within which human vWF (10 μg/ml) was immobilized and a shear rate of 1,600 s⁻¹ was applied. imMKCL platelets showed 62.3% (Cl-2) and 75.8% (Cl-7) of the CD42b-dependent binding of fresh human platelets, and human CD42b blocking antibody reversed this adhesion (Figure 5F). With our current protocol, final platelet collection takes place during the final 5 days in the absence of serum at 37°C. Altogether, these two conditions may account for the relatively low granule content (Figure S6C) and diminished aggregation (Figure 5D).

electron microscopy revealed frequent generation of platelets through cytoplasmic fragmentation (Figure S6A) and proplatelets in the culture dish (Figure 3C and Movie S1). Individual imMKCL-derived platelets showed normal microtubules but fewer granules when compared to fresh human donor platelets (Figure 5A and S6A). To explore the functionality of imMKCL-derived platelets, we used flow cytometry to examine integrin αIIbβ3 activation (inside-out signaling) or platelet aggregation after stimulation with platelet agonists (De Cuyper et al., 2013). Agonist stimulation increased PAC-1 binding mean fluorescent intensity, given that this antibody binds to the activated form of αIIbβ3 integrin (Figures 5B and 5C) as well as platelet aggregation (Figure 5D), clot retraction (Figure 5E), actin cytoskeletal changes (Figure S6B), and vWF or ADP secretion (Figure S6C). Collectively, most in vitro functional parameters indicated that imMKCL platelets gave less robust responses than fresh human platelets, but, comparison to pooled human endogenous platelets (Figures 5C and 5D) or iPSC-derived platelets generated

imMKCL-Derived Platelets Show Thrombogenic Activity in Mouse Models of Thrombocytopenia

Next, we evaluated the in vivo circulation of imMKCL platelets with previously optimized transfusion models (Takayama et al., 2010). Using NOD/SCID/IL-2Rg-null (NOG) mice with irradiation-induced thrombocytopenia, flow cytometric analyses were carried out 30 min, 2 hr, and 24 hr after transfusion (1 or 6 × 10⁸ platelets per mouse). The posttransfusion kinetics of imMKCL-derived platelets were nearly the same as those obtained with fresh human platelets (n = 4 individual groups in two independent experiments; Figures 6A and 6B). To further assess the functionality of imMKCL platelets in vivo, we used
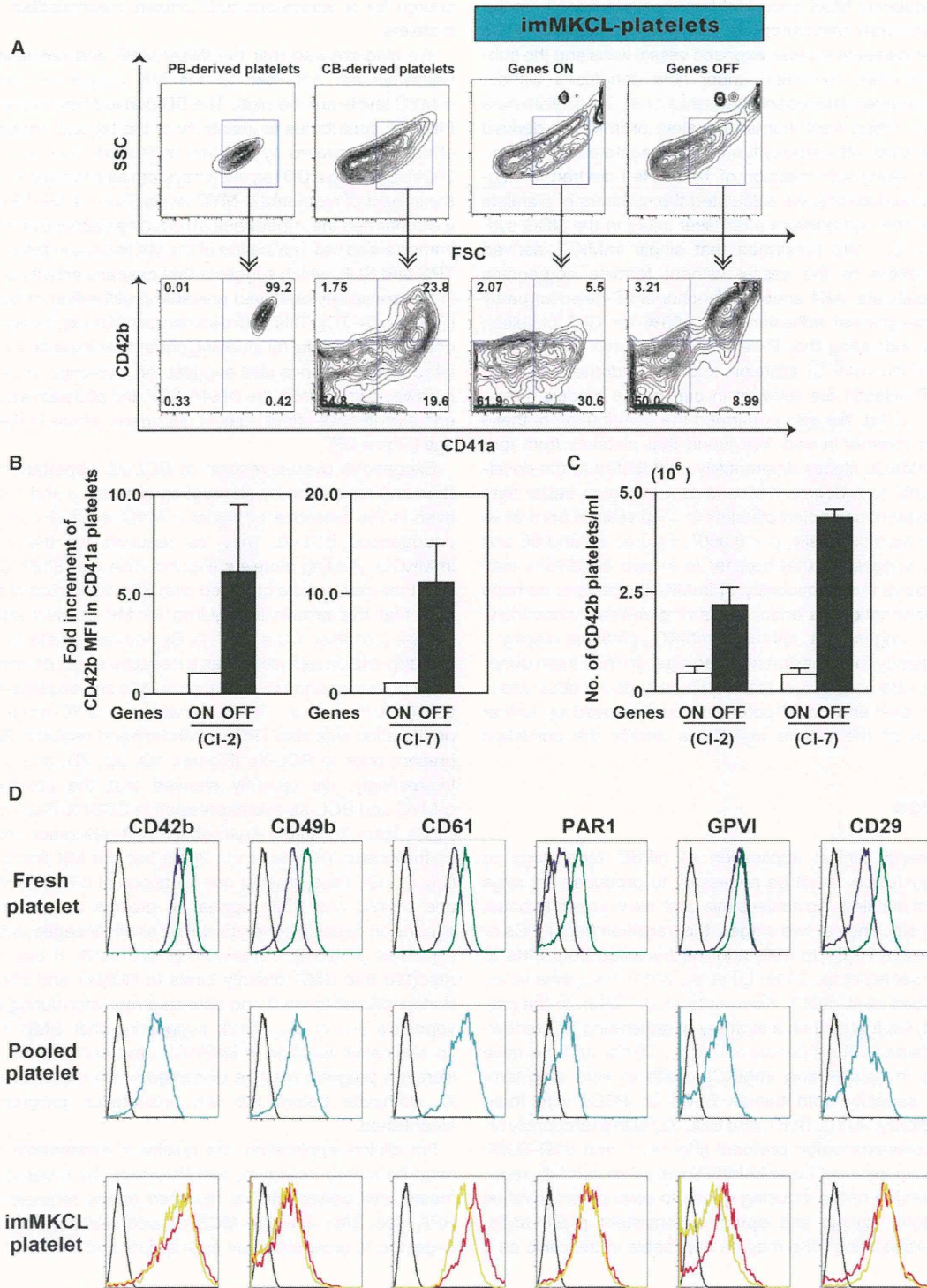
Figure 4. imMKCL-Derived Mature MKs Generated CD41a⁺CD42b⁺ Platelets upon Turning Off 3F Transgenes

(A) Representative contour plots for human peripheral blood (PB)-, CB-CD34⁺HS/PC-, and imMKCL (3F on and off)-derived platelets (platelet population are shown in side and forward scatter contour plots).

(B) Fold increment in CD42b⁺ mean fluorescent intensity (MFI) among CD41a⁺ imMKCL Cl-2 (KhES3)- and Cl-7 (DN-SeV2)-derived platelets. White bars, genes on; black bars, genes off. Results are expressed as means± SE from three independent experiments. The mean value of the samples with genes on is assigned as 1.0.

(legend continued on next page)

Cell Stem Cell *14*, 1–14, April 3, 2014 ©2014 Elsevier Inc.